Kinematic Framework for Evaluating Seismic Earth Pressures on Retaining Walls

by

Scott J. Brandenberg[1], **M. ASCE**, George Mylonakis[2], **M. ASCE**, and Jonathan P. Stewart[3], **F. ASCE**

Abstract: During earthquake ground shaking earth pressures on retaining structures can cyclically increase and decrease as a result of inertial forces applied to the walls and kinematic interactions between the stiff wall elements and surrounding soil. The application, based on limit equilibrium analysis, of a pseudo-static inertial force to a soil wedge behind the wall (the mechanism behind the widely-used Mononobe-Okabe method) is a poor analogy for either inertial or kinematic wall-soil interaction. This paper demonstrates that the kinematic component of interaction varies strongly with the ratio of wavelength to wall height (λ/H), asymptotically approaching zero for large λ/H, and oscillating between the peak value and zero for $\lambda/H < 2.3$. Base compliance, represented in the form of translational and rotational stiffness, reduces seismic earth pressure by permitting the walls to conform more closely to the free-field soil displacement profile. This framework can explain both relatively low seismic pressures observed in recent experiments with $\lambda/H >$ ~10, and relatively high seismic earth pressures from numerical analyses in the literature with $\lambda/H = 4$.

Keywords: wall, seismic earth pressure, wave, analysis, dynamic testing

[1] Associate Professor and Vice Chair, Department of Civil and Environmental Engineering, 5731 Boelter Hall, University of California, Los Angeles, CA 90095-1593. Email: sjbrandenberg@ucla.edu.
[2] Professor and Chair in Geotechnics and Soil-Structure Interaction, Department of Civil Engineering, University Walk, Clifton BS8, University of Bristol, UK; Professor, University of Patras, Greece; Adjunct Professor, University of California, Los Angeles. Email: g.mylonakis@bristol.ac.uk.
[3] Professor and Chair, Department of Civil and Environmental Engineering, 5731 Boelter Hall, University of California, Los Angeles, CA 90095-1593. Email: jstewart@seas.ucla.edu.

Introduction

The increment of lateral earth pressure that should be applied during the design of retaining walls to account for earthquake effects has been a source of confusion among design professionals and a topic on which there are divergent opinions among researchers. Current guidelines documents (*e.g.*, NCHRP, 2008) prescribe substantial seismic earth pressures beyond those for the pre-seismic (generally active) condition. These recommendations are based on a limit equilibrium analysis in which a pseudo-static seismic coefficient (k_h) acts upon an active Coulomb-type wedge in frictional soil, which in turn results in an incremental change in the lateral force applied to the wall, P_{AE}, over its static counterpart P_A. This approach is based on the classical work by Okabe (1924) and Mononobe and Matsuo (1929) [widely known as the "Mononobe-Okabe" (M-O) method] with modest modification by Seed and Whitman (1970). More accurate variants on the classical approach using non-planar failure surfaces (Chen, 1975; Chen and Liu, 1990) and approximate accounting for the phasing of inertial demands within the wedge (Steedman and Zeng, 1990) are conceptually alike and provide similar results for the active case.

Recent work based on experiments and various dynamic solutions considering elastic soil behavior has, directly or indirectly, challenged this practice as being both too conservative (e.g., Al Atik and Sitar, 2010; Lew et al., 2010) and as being un-conservative (e.g., Wood 1973, Veletsos and Younan 1994, Ostadan, 2005). These conflicting findings, based on different approaches and assumptions regarding system behavior, drive a good deal of the confusion on the subject of seismic earth pressures on retaining walls. A fundamental problem is that the M-O method does not adequately represent interaction of vibrating soil in the free field with an embedded structure or a retaining wall. This interaction may be best understood using a conceptual framework, rooted in the principles of soil-structure interaction and wave propagation, in which kinematic and inertial interaction effects are distinguished.

The next section describes a conceptual framework for defining seismic earth pressures from kinematic interaction in terms of the ratio of wavelength of vertically propagating shear waves to wall height. This approach convincingly explains the apparently divergent findings from centrifuge tests by Al Atik and Sitar (2010) and the numerical results from Ostadan (2005). Recommendations for rational simplified analysis of seismic earth pressures in engineering practice are then presented, along with conditions for which more elaborate analyses are needed.

Conceptual Framework

The seismic increment to lateral earth pressures can be considered as having kinematic and inertial components, as illustrated in Figure 1 for an embedded building foundation with relatively stiff basement walls. The free-field motion imposed on this system (u_g) varies with depth as indicated in Figure 1(a). In the kinematic problem for which there is no structure or wall inertia, the motion of the foundation at base depth H is denoted u_{FIM} (FIM is "foundation input motion"), which differs from the free-field motion at this same depth, $u_g(H)$, as a result of relative foundation/free-field displacements associated with wall-soil contact stresses, as well as base slab averaging effects that occur in the presence of inclined or incoherent waves (e.g., Veletsos and Prasad, 1989). The kinematic component of seismic earth pressures accounts for the interaction between the free-field motion $u_g(z)$ and the structural wall elements, apart from their inertia and any external inertial loads imposed upon the system.

As shown in Figure 1(b), the inertial interaction problem involves computation of the response of a structure and its foundation to the kinematic ground motions. Inertial forces from the structure cause additional relative displacements between the foundation and the free-field, and additional increments of seismic earth pressure. The springs and dashpots in Figure 1(b) represent the impedance of the foundation from translation and rocking vibration modes (*e.g.*, Pais and Kausel, 1988; Gazetas, 1991).

In light of the above soil-structure interaction framework, the soil wedge concept currently used to evaluate seismic earth pressures will seldom have relevance to the physical mechanisms producing those pressures. Even in cases where a state of active earth pressure (and its associated soil wedge) exists prior to seismic shaking, increments of earth pressure from earthquake ground shaking will arise from relative displacements between the wall and free-field soil associated with kinematic and inertial interaction, which is not well represented by a seismic coefficient acting on an active wedge. Inertial interaction can mobilize large relative displacements when, for example, a massive structure is connected to the wall elements and base shear mobilizes reaction stresses at the soil/wall interface. Such effects can be evaluated as part of seismic structural response analysis if soil springs are included in the structural model. Free-standing walls or basement walls not structurally connected to lateral force resisting elements in structures would have seismic earth pressures dominated by kinematic interaction, which is the topic addressed in the remainder of this article.

Model Derivation

Seismic earth pressures arising from kinematic interaction are formulated based on the following assumptions (Fig. 2): (1) an infinitely long U-shaped structure with rigid walls and rigid base slab is embedded in a soil profile with a uniform shear wave velocity, (2) a vertically propagating shear wave interacts with the embedded structure, (3) the soil and wall are in perfect contact, and a gap does not form at this interface, and (4) the interaction between the soil and vertical walls is characterized by stiffness intensity terms, k_y^i and k_z^i (defined below), and interaction between the soil and base slab is characterized by stiffness terms K_y and $K_{xx,base}$. These stiffness terms satisfy the Winkler assumption that the stiffness values act independently from one another, which is a simplifying assumption commonly used in soil-structure interaction problems because it permits development of tractable solutions. The values assigned to the stiffness terms should account for coupling between various foundation vibrations modes, as described later. Although these assumptions may appear to be limiting, the method can be readily extended to a wide range of practical conditions (including non-rigid foundations as well as non-linear and non-uniform soil) in a manner typical of soil-structure interaction applications (NIST, 2012) as illustrated subsequently.

The model derivation is described in two stages. *First*, wall pressures and their resultant demands (forces and moments) are derived from the product of differential wall/free-field displacement and wall-soil stiffness. *Second*, equations for the stiffness terms are developed, which is essential for analysis of force/moment demands and differential wall/free-field motions. Fundamental characteristics of wall-soil interaction derived from these analyses are then described and illustrated using example solutions, which demonstrate that the wall-soil interaction response depends strongly on the ratio of wavelength to wall height.

Wall-Soil Interaction Forces and Displacements

A rigid U-shaped structure with vertical walls embedded in a soil profile experiencing vertically propagating harmonic free-field shear waves is shown in Figure 2. Note that the free-field ground motion is consistent with the influence of the free-surface since the shear strain is zero at z=0.

Kinematic wall pressures arise from incompatibility in the displacement of the rigid wall and the free-field soil column. Accordingly, the integral of the horizontal stress increment over the height of the wall is the kinematic seismic force increment P_E (P_E is adopted here instead of P_{AE}, which is associated with M-O theory, because our solution does not require an active condition). For ground motion in the y-direction, P_E is calculated as a force per unit length as follows:

$$P_E = \int_0^H k_y^i \left(u_{g0} \cos kz - u_w(z) \right) dz \tag{1}$$

where H = wall height, $u_w(z)$ = wall displacement at depth z, k_y^i = soil-wall reaction stiffness in y-direction (normal stresses) per unit of wall area (superscript i denotes stiffness intensity measured in units of F/L^3; details below), $k=2\pi/\lambda$ = wave number, and λ = wavelength of the shear wave propagating vertically through the soil. The moment applied by the horizontal soil-wall interaction stresses relative to the foundation slab base elevation is:

$$M_E = \int_0^H k_y^i \left(H - z \right) \left(u_{g0} \cos kz - u_w(z) \right) dz \tag{2}$$

Equations (1) and (2) can be combined to calculate the location of resultant P_E, measured as distance h upwards from the base of the wall as:

$$\frac{h}{H} = \frac{M_E}{P_E H} \tag{3}$$

The depth-dependent wall displacement $u_w(z)$ for a rigid wall and foundation system is:

$$u_w(z) = u_{FIM} + \theta_{FIM}\left(H - z\right) \tag{4}$$

where u_{FIM} and θ_{FIM} are the base slab translation and rotation, respectively.

For a rigid wall resting on a rigid base, θ_{FIM} must be zero, base displacement must equal free-field displacement at the base of the wall (i.e., $u_{FIM} = u_{g0}\cos kH$), and the solution for P_E, and M_E may easily be obtained from Eqs. 1 and 2 for a free-field ground motion with any particular wavelength. However, a more general solution for a wall embedded within an elastic layer, thereby exhibiting base compliance, can also be obtained. The rotational stiffness of the embedded strip contains contributions from the base slab and from vertical shear tractions and horizontal normal stresses acting on the walls. The horizontal stresses acting on the walls are explicitly included in Eqs. (1) and (2). The base slab and vertical traction contributions are combined as $K_{xx} = K_{xx,base} + 2k_z^i HB^2$.

To solve for the foundation input motions, horizontal force and moment equilibrium of the foundation slab are considered, assuming that the free-field ground motion is input to the free-ends of the soil-structure interaction elements. Substituting (4) into (1) and (2), and requiring horizontal force and moment equilibrium between the wall resultants and base reactions provides:

$$P_E = \int_0^H k_y^i\left[u_{g0}\cos kz - u_{FIM} - \theta_{FIM}\left(H - z\right)\right]dz = \frac{K_y}{2}\left[u_{FIM} - u_{g0}\cos kH\right] \tag{5a}$$

$$M_E = \int_0^H k_y^i\left[u_{g0}\cos kz - u_{FIM} - \theta_{FIM}\left(H - z\right)\right]\left(H - z\right)dz = \frac{K_{xx}\theta_{FIM}}{2} \tag{5b}$$

Stiffness terms K_y and K_{xx} are multiplied by ½ to account for two vertical walls being attached to a single rigid base. By evaluating the integrals and re-arranging terms, the following solution is obtained for foundation displacements:

$$H_u = \frac{u_{FIM}}{u_{g0}} = \frac{\left(6H^2\left(k_y^i\right)^2 + 3k^2K_yK_{xx} + 2k^2H^3K_yk_y^i\right)\cos kH + \left(4kH^3\left(k_y^i\right)^2 + 6kK_{xx}k_y^i\right)\sin kH - 6H^2\left(k_y^i\right)^2}{k^2\left(H^4\left(k_y^i\right)^2 + 2H^3K_yk_y^i + 6HK_{xx}k_y^i + 3K_yK_{xx}\right)} \tag{6a}$$

$$H_\theta = \frac{\theta_{FIM}B}{u_{g0}} = B\frac{\left(6k^2H^2K_yk_y^i + 24H\left(k_y^i\right)^2 + 12K_yk_y^i\right)\sin^2(kH/2) - 6kH^2\left(k_y^i\right)^2\sin kH - 3H^2k^2K_yk_y^i}{k^2\left(H^4\left(k_y^i\right)^2 + 2H^3K_yk_y^i + 6HK_{xx}k_y^i + 3K_yK_{xx}\right)} \tag{6b}$$

These foundation displacements can then be inserted into Eq. (5) to obtain P_E and M_E for a compliant base condition.

Stiffness of Wall-Soil System

Having formulated the solution for P_E and M_E, the stiffness terms, k_y^i, k_z^i, K_y, and $K_{xx,base}$, are now evaluated. Classical inertial SSI literature (e.g., summarized by Gazetas 1983, Mylonakis et al. 2006, and NIST 2012) provides equations for the overall stiffness of embedded foundations representing the interaction of the soil with the entire foundation system, but the global stiffness is not partitioned into contributions from the vertical walls and the base slab. Such partitioning is required to obtain the distribution of earth pressure acting on the vertical walls, which is the objective. To overcome this problem, available solutions are first used to define stiffness terms for individual foundation components under the assumption of no interaction between vibration modes (i.e., the components are independent). Next, modification factors χ_y and χ_{xx} are introduced to account for interaction between the translation and rotation terms, respectively, such that the resulting global foundation stiffness matches published equations for embedded foundations. For simplicity, the base and wall stiffnesses are both modified by the same χ_y and χ_{xx} terms.

Horizontal wall-soil stiffness intensity k_y^i

Kloukinas et al. (2012) developed a simple analytical expression for k_y^i for kinematic interaction between rigid vertical walls and an elastic soil layer resting atop a rigid base. Following correction of their published expression (a clerical error involving omission of the square root in the denominator) and including the multiplier, χ_y, we obtain the stiffness intensity as:

$$k_y^i = \chi_y \frac{\pi}{\sqrt{(1-\nu)(2-\nu)}} \frac{G}{H} \sqrt{1-\left(\frac{2\omega H}{\pi V_s}\right)^2} \tag{7a}$$

where ω is angular frequency (rad/sec). Material damping can be incorporated into the solution by using complex shear modulus, $G(1+\mathbf{i}2\xi)$, and complex shear wave velocity, $V_s(1+\mathbf{i}\xi)$, where ξ is percent material damping. Kloukinas et al. (2012) develop kinematic earth pressures for a rigid wall resting atop a rigid base, whereas our solution corresponds to soil profiles that are deeper and compliant under the wall, which is applicable to more realistic conditions. For an ideally undamped medium, the square root on the right-hand side of Eq. (7a) can be interpreted as a dynamic stiffness modifier (often denoted by α) that accounts for frequency-dependence from soil inertia, with the corresponding dashpot equal to zero. At $\omega = \pi V_s / 2H$ the dynamic modifier becomes zero and at higher frequencies k_y^i becomes imaginary meaning that the spring acts as a dashpot. This phenomenon is directly related to the rigid base condition used in the solution, which only allows radiation damping (from wave propagation away from the foundation) beyond the "cutoff frequency" (e.g., Elsabee and Morray, 1977). For realistic systems involving a compliant base condition, the cutoff frequency transition is smoother, allowing waves to exist at a wider range of frequencies (Li, 1999), and material damping results in non-zero real and imaginary components at all frequencies. Elsabee and Morray (1977) suggest simple expressions for handling these problems for embedded circular foundations, but there is presently no simple solution analogous to Eq. (7a) to account for these effects for two-dimensional vertical walls.

Vertical wall-soil stiffness intensity k_z^i

Following the method of Kloukinas et al. (2012), the digital supplement presents the derivation of an expression for stiffness intensity associated with vertical tractions acting on walls (soil-wall reaction stiffness in *z*-direction from shear), k_z^i. The resulting expression is given below along with a multiplier, χ_{xx}, that modifies the vertical stiffness to account for interaction associated with base rotation and translation:

$$k_z^i = \chi_{xx} \frac{\pi}{2} \sqrt{\frac{2-\nu}{1-\nu}} \frac{G}{H} \sqrt{1 - \left(\frac{2\omega H}{\pi V_s} \right)^2} \tag{7b}$$

Base slab stiffness terms K_y and $K_{xx,base}$

Gazetas and Roesset (1976) developed simple analytical expressions for the translational and rotational stiffness (K_y and $K_{xx,base}$, respectively) of a rigid strip footing resting on the surface of a homogeneous elastic layer of finite thickness overlying a rigid base. Applying the interaction constants χ_y and χ_{xx} and adjusting the soil thickness term to be equal to the distance from the base slab to the rigid base (i.e., using *D*-*H*), results in:

$$K_y = \chi_y \frac{2.1G}{2-\nu}\left(1+2\frac{B}{D-H}\right), \quad K_{xx,base} = \chi_{xx} \frac{\pi GB^2}{2(1-\nu)}\left(1+\frac{1}{5}\frac{B}{D-H}\right) \tag{8a, 8b}$$

It should be noted that the solution in Eq. (8a) does not extrapolate properly to an infinitely thick elastic layer, for which the stiffness of a strip footing is zero. On the other hand, under such a condition the solution in Eq. (8b) is exact (Mushkelishvili, 1963).

Derivation of interaction terms χ_y and χ_{xx}

The above component stiffnesses can be combined to compute overall static stiffnesses for the embedded wall-soil system in translation and rocking. For translation, the stiffness is $2k_y^iH + K_y$, which includes contributions from the vertical walls and the base slab. For rotation, the stiffness is $k_y^iH^2 + K_{xx,base} + 2k_z^iHB^2$, which includes contributions from horizontal and vertical earth pressures acting on the vertical walls and the rotational stiffness of the base slab.

Values of χ_y and χ_{xx} were selected such that the global stiffness of the foundation matches the equations for embedded strip footings by Jakub and Roesset (1977):

$$K_{y\_emb} = \frac{2.1G}{2-\nu}\left(1+2\frac{B}{D}\right)\left(1+\frac{1}{3}\frac{H}{B}\right)\left(1+\frac{4}{3}\frac{H}{D}\right) = 2k_y^iH + K_y \tag{9a}$$

$$K_{xx\_emb} = \frac{\pi GB^2}{2(1-\nu)}\left(1+\frac{1}{5}\frac{B}{D}\right)\left(1+\frac{H}{B}\right)\left(1+\frac{2}{3}\frac{H}{D}\right) = k_y^iH^2 + K_{xx,base} + 2k_z^iHB^2 \tag{9b}$$

Expressions for χ_y and χ_{xx} can be obtained by substituting Eqs. (7) and (8) into (9). Figure 3 presents the values of χ_y and χ_{xx} versus *H/B* for various values of *D/H*. The solutions by Jakub and Roesset are intended for conditions in which D/B > 2 and H/B < 2/3, and may provide erroneous results for conditions outside these bounds. Extrapolation is bounded by the Kloukinas et al. (2012) solution for D/H=1, in which case χ_y = 1.0, and the halfspace solution when $D/H \rightarrow \infty$, in which case χ_y = 0.0. These bounds are presented in Fig. 3, and interpolation from the figure is recommended for D/H<2 and D/H>20 rather than the values of χ_y and χ_{xx} implied by Eqs. (7)-(9).

Characteristics of Wall-Soil Interaction Response

Figure 4 shows solutions for P_E computed using Eq. (5a) with the expression for foundation input motion given in Eqs. (6). Results are plotted for various values of $K_y/(k_y^i H)$ and $K_{xx}/(k_y^i H^2/3)$ (representing the relative contributions of the base slab and horizontal normal stresses acting on the walls to horizontal and rotational stiffness, respectively). In addition to the cases with a compliant base, a rigid base case (K_y and $K_{xx} \rightarrow \infty$) is included for comparison. For a given λ/H, the highest values of P_E occur for the rigid base case. P_E decreases as K_y and K_{xx} decrease because a more flexible base condition results in less relative displacement between the wall and free-field soil along the wall height.

The most important interval of λ/H in Figure 4 for application to typical structural configurations and earthquake ground motions is the portion to the right of the longest wavelength (lowest frequency) peak in P_E, which occurs at $\lambda/H \approx 2.3$. The importance of this interval stems from its likely proximity to energetic portions of the ground motion spectrum, which occur at the site resonant frequency or at frequencies controlled by the seismic source and path (which are typically higher than the site frequency for sites in sedimentary basins).

To support the assertion that the important portion of the plot is typically $\lambda/H \geq 2.3$, consider first the case of free field seismic energy that is dominated by site resonance. The site resonant frequency corresponds to λ/D = 4, which can be manipulated to λ/H=4D/H. Since the thickness of the soil column generally significantly exceeds the wall height (i.e., generally D » H), λ/H will typically exceed 4, which falls well to the right of the lowest frequency peak at $\lambda/H \geq 2.3$. For this resonant condition, the largest kinematic pressures occur when D=H (i.e., base slab is founded on stiff rock overlain by soil).

Free-field ground motions are often not dominated by a fundamental-mode site response, particularly in sedimentary basins where seismic velocities gradually increase with depth without having a distinct impedance contrast. In such cases, the controlling ground motion period can be estimated as the mean period (T_m = period at the centroid of the Fourier amplitude spectrum), which is typically in the range of 0.3 to 0.5 sec for earthquakes in active crustal regions in the magnitude range of engineering interest (Rathje, et al., 2004). The corresponding wavelenths (computed as $\lambda = V_sT_m$) will seldom place the applicable value of λ/H below the peak at ~2.3 for typical values of wall height H.

Based on the above considerations, the most useful insights into kinematic wall pressures are gained by studying the portion of the results in Figure 4 for $\lambda/H > \sim 2.3$. Kinematic pressures are clearly high near the peak at 2.3 due to large relative deformations of wall and soil. As λ/H increases beyond 2.3, P_E decreases rapidly. In the limiting case where $\lambda/H \rightarrow \infty$, the deformed shape of the free-field soil profile would become vertical and would precisely conform to the shape of the rigid wall, thereby resulting in zero kinematic interaction. The peaks and troughs in P_E observed for λ/H < 2.3 are caused by alternation of the direction of the horizontal stress increment acting along the wall height as frequency changes.

Figure 5 shows kinematic transfer functions H_u and H_θ associated with the solution for the foundation input motion (Eq. 6). The transfer functions are compared to the recommendation by Kausel et al. (1978), who used an embedded cylinder geometry, assumed $u_{FIM} = u_g(H)$ (this is the same as assuming $K_y \rightarrow \infty$), and approximated high frequency interaction (i.e., at low λ/H) as constant with respect to frequency for simplicity. At large λ/H, the H_u values for the rigid base case agree perfectly with Kausel et al., whereas base compliance results in increased translation and rotation. The assumption that $u_{FIM} = u_g(H)$ is approximate, even in the presence of vertically propagating coherent waves, due to the wall-soil interaction force P_E that must be balanced by deflection of the base slab. As H/B increases, translation amplitude decreases and rotational amplitude increases for a particular λ/H.

Recommended Methods of Implementation

The solution for P_E in Eq. 5a is a function of wave number, k, and is therefore a function of frequency. The dependence of P_E on frequency can be captured with two methods: (1) a frequency-domain solution that takes as input a time-series of free-field ground surface displacement [$u_{g0}(t)$], or (2) a single-frequency solution that takes as input a particular free-field displacement (u_{g0}) and a single frequency anticipated to dominate dynamic earth pressure response. Both methods will be useful in design applications and are described below.

The frequency domain solution (FD solution) has the following steps:

1) Compute the Fourier transform of the free-field ground displacement record, $\hat{u}_{g0}(\omega)$ using a fast Fourier transform algorithm.

2) Compute frequency-dependent values of the stiffness parameters k_y^i, k_z^i, K_y, and $K_{xx,base}$ using Eqns. (7)-(9). Follow typical protocols (NIST, 2012) for selecting representative shear moduli for use in these expressions, including averaging non-uniform shear-wave velocities over appropriate depth ranges and using applicable levels of modulus reduction for nonlinear problems (described further below). Alternative values for embedded foundation stiffness to those given in Eqs. (9), as derived from site- and structure-specific analysis or from alternate solutions in the literature, can be readily incorporated by entering the computed values for K_{y_emb} and K_{xx_emb}. This could be particularly important for foundation geometries that are not well approximated as plane strain for a particular direction of shaking [e.g., rectangular foundations, for which impedance solutions are available in Gazetas (1983), Mylonakis et al. (2006) and NIST (2012)]. Material damping may also be incorporated through the use of complex-valued shear moduli as noted above.

3) Compute the Fourier coefficients of the frequency-dependent foundation input motions $\hat{u}_{FIM}(\omega)$ and $\hat{\theta}_{FIM}(\omega)$ using Eqs. 6a and 6b. Note that $\hat{u}_{g0}(\omega)$ is substituted for u_{g0} in these equations for the frequency domain solution.

4) Compute the Fourier coefficients of the seismic earth pressure resultant, $\hat{P}_E(\omega)$, using Eq. 5a. Note that $\hat{u}_{g0}(\omega)$, $\hat{u}_{FIM}(\omega)$ and $\hat{\theta}_{FIM}(\omega)$ are substituted for u_{g0}, u_{FIM}, and θ_{FIM}, respectively.

5) Compute the time series of the seismic earth pressure resultant, $P_E(t)$ using the inverse fast Fourier transform algorithm. Find the maximum value of this time series. The total demand on the wall is the sum of P_E (at the location indicated by Eq. 3) and the resultant of the initial earth pressure (typically at $z = 2H/3$).

Each of the frequency-domain displacements and forces given above is complex valued.

The single-frequency solution (SF solution) is as follows:

i. Estimate the mean period (T_m) of the design earthquake ground motion. For projects where ground motions are estimated using site-specific probabilistic seismic hazard analysis followed by the selection of applicable accelerograms, the mean period can be computed for each record using procedures given in Rathje et al. (2004). When such accelerograms are unavailable, T_m can be computed from applicable ground motion prediction equations (*e.g.*, Rathje et al., 2004), or in cases of sites having significant impedance contrasts giving rise to strongly resonant responses, from the site period $\left(T = 4H/V_s\right)$.

ii. Compute k_y^i, k_z^i, K_y, and $K_{xx,base}$ using Eqns. (7)-(9) or alternate solutions as described in Step (2) above. For many practical situations, static stiffnesses will suffice for these quantities (zero frequency), although more precision is possible through consideration of frequency dependence.

iii. Use the results in Fig. 4, or a site-specific solution of Eq. (5), to evaluate the variation of normalized P_E [i.e., $\left|P_E\right| / \left(u_{g0} k_y^i H\right)$] versus λ/H.

iv. Compute λ/H, based on the mean period from Step *(i)* (*i.e.*, $\lambda/H = V_S T/H$), and compute the associated normalized value of P_E. Kinematic interaction is anticipated to be significant if the wall under consideration lies near the fundamental-mode peak response region (i.e., $\lambda/H \approx 1.5$ to 4), and small in regions of lower frequency (e.g., $\lambda/H > \sim 10$).

v. Estimate u_{g0} so that the dimensionless wall force from (*iv*) can be dimensionalized. Ground motion amplitude u_{g0} should not be perceived as the peak ground displacement, but rather as a displacement associated with the most energetic portion of the record.

Until more detailed validation exercises can be performed, u_{g0} should be taken as PGV/ω_m, where PGV is the peak ground velocity in the free field and ω_m is the angular mean frequency corresponding to the mean period from (1) ($\omega_m = 2\pi/T_m$). Energetic portions of the ground motion spectrum are correlated with PGV (e.g., Akkar and Özen, 2005; Bommer and Alarcón, 2006).

vi. The total demand on the retaining wall is computed from P_E and the resultant of the initial earth pressure, as in the FD procedure.

Several important issues arise when selecting a representative shear wave velocity using either the FD or SF solutions. First, shear wave velocity typically varies with depth due to pressure-dependence of soil shear modulus and age. For computing k_y^i and k_z^i, the time-averaged shear wave velocity (depth/travel time) for the depth interval from the ground surface to the bottom of the wall should be used. For computing base stiffness terms, the time-averaged shear wave velocity for the depth interval from $z = H$ to $H+B$ should be used, until more detailed recommendations can be developed.

Second, strong ground motion induces shear strains that are large enough to reduce the secant shear modulus in accordance with a modulus reduction curve. Failing to account for modulus reduction may result in a significant over-prediction of earth pressure since the reduction in secant shear modulus reduces k_y^i, k_z^i, K_y, and $K_{xx,base}$. A site-specific ground response analysis is recommended to obtain values of strain-compatible shear modulus (and associated equivalent-linear V_s). An alternative crude approach is to approximate the peak shear strain based on PGV/V_s. Assuming the standing wave field in Fig. 2 varies in time according to $u_g(z,t) = u_{g0}\cdot\cos(kz)\cdot e^{i\omega t}$, the ground surface velocity is $du_g(0,t)/dt = \dot{u}_{g0} = i\cdot\omega\cdot u_{g0}\cdot e^{i\omega t}$ and the shear strain is $du_g/dz = -k\cdot u_{g0}\cdot\sin(kz)\cdot e^{i\omega t}$. Therefore the strain field is $du_g/dz = (\dot{u}_{g0}/V_s)\cdot i\cdot\sin(kz)$, the amplitude of which is simply PGV/V_s. The imaginary number indicates that shear strain is 90° out of phase with surface velocity. Furthermore, the maximum values of shear strain occur at the "nodes" of the standing wave (i.e., at $kz = \pi/2 + n\pi$, where n is an integer greater than 0). For more complicated conditions including soil layering and propagation of surface waves, shear strain has been found to range from 0.2 to 1.7 times PGV/V_s, with 1.0 being a commonly used value for horizontal-component ground motions (Trifunac et al., 1996; Brandenberg et al., 2009), which provides an estimate of peak shear strain consistent with the assumed shape of the soil displacement profile. This peak shear strain can then be converted to a representative uniform strain by multiplying the peak shear strain by (**M**-1)/10, where **M** is moment magnitude (Idriss and Sun, 1991). The equivalent uniform shear strain would then be used to compute a value of G/G_{max} from a selected modulus reduction curve, from which reduced values of G and V_s can be obtained for use in the analysis. This equivalent-linear procedure neglects local strains imposed by the wall, and is reasonable for cases involving free-field ground strains smaller than about 1%. However, the procedure may become erroneous at larger strains corresponding to ground failure. Free-standing retaining walls that rotate or translate significantly may mobilize such large shear strains, but this will rarely be the case for stiff building basement walls.

The solution presented herein assumes perfect contact between the soil and the vertical walls. In reality, a gap might form in cohesive soils at this interface if P_E is negative (i.e., the wall is moving away from the soil) and its absolute value is larger than the initial earth pressure on the wall. Gapping may theoretically cause pounding and additional stresses on the wall beyond those considered here. However, it is likely that peak earth pressures will occur when P_E is positive (i.e., when the free-field soil moves toward the wall), which is considered in the present analysis.

The efficacy of the proposed procedure is demonstrated in the following section and will be tested further over time as additional experimental data become available.

Comparison to Experimental- and Simulation-Based Results in Literature

In this section, two prior studies that reached strongly divergent conclusions about the levels of seismic earth pressures acting on retaining walls are interpreted using the proposed methodology. In the first study, Ostadan (2005) performed elastic wave propagation analysis using a numerical finite element code (SASSI; Lysmer et al. 1999) to investigate the kinematic interaction between free-field site response and a massless embedded structure connected to a rigid base and fixed against rotation. Ostadan concluded that M-O earth pressure theory significantly under-predicts the mobilized earth pressures by factors ranging from 2 to 4 depending on ground motion characteristics. In the second study, Al Atik and Sitar (2009) performed centrifuge modeling of embedded U-shaped walls, and concluded that M-O theory significantly over-predicts measured earth pressures. On the basis of their test results, they reported that dynamic earth pressures driving flexural demands on the walls are negligible for peak horizontal surface accelerations less than 0.4g.

Ostadan (2005) Numerical Solution

Ostadan (2005) input six broadband earthquake motions, scaled to a common peak horizontal acceleration of 0.3g, to the base of an elastic soil layer with V_s = 305 m/s, H = 9.14m, mass density ρ=2.06Mg/m^3, ν=1/3, and ξ=5%. The elastic layer rests atop a rigid base. This elastic layer is the backfill behind a rigid wall also supported on the rigid base. The ground motions generated substantial site response due both to the infinite impedance contrast (from the rigid base) and significant energy in the input motions at the fundamental frequency of the backfill (where λ/H=4).

Five of the free-field surface motions were obtained from Ostadan (*pers. communication*, 2013) and used to compute $u_{g0}(t)$ by double-integrating the surface accelerations in time. Those free-field motions were then applied using the proposed FD and SF solutions. Since the base of the wall was rigidly connected to the ground, only the stiffness term k_y^i is needed in the solution, and the frequency-dependent value was computed using Eq. (7a) with χ_y = 1. Figure 6a compares maximum earth pressures over the wall height from the FD solution relative to those obtained by Ostadan (2005) for two of the ground motions (three are omitted for clarity in the figure). Table 1 presents the resultants of these distributions. The resultant forces are in good agreement, with errors ranging from -10% to +12%.

In the SF solution, the surface displacement is computed as $u_{g0}=PGV \cdot T/2\pi$, where PGV is taken from ground-surface motions, and period T is taken as $4H/V_s$ due to the strong impedance contrast at the base of the soil layer. The agreement with Ostadan's solution is reasonable, but not as good as the FD solution, with errors ranging from -12% to +57%. The Mononobe-Okabe earth pressure resultant presented by Ostadan (160 kN/m for all of ground motions) underpredicts the earth pressures in every case.

The conditions considered by Ostadan are nearly optimal for generating large kinematic wall pressures (i.e., λ/H = 4, associated with first mode response of the backfill, lies near the peaks of the curves in Fig. 4). Not surprisingly, such conditions cause the mobilized earth pressures to exceed those from the M-O theory. Ostadan's results are broadly consistent with earlier findings by Arias et al. (1981) and Veletsos and Younan (1994) obtained by analytical closed-form solutions for similar configurations.

Al Atik and Sitar (2009, 2010) Experimental Results

Al Atik and Sitar (2009, 2010) performed centrifuge experiments on relatively rigid and flexible U-shaped walls with prototype dimensions of H = 6.5 m and B = 5.3m embedded in a profile of medium dense sand with thickness D = 19 m, and γ = 17 kN/m^3. The average small-strain shear wave velocities given by Al Atik and Sitar were V_s = 170 m/s behind the walls and V_s = 260 m/s for the depth interval from the base of the wall to the essentially rigid base of the container. The FD and SF solutions are compared with results of experiments performed using motions denoted Loma Prieta SC1, Loma Prieta SC2, and Kobe PI2.

For these experiments, u_{g0} was obtained by digitizing and double-integrating in time the plots of free-field surface acceleration presented by Al Atik and Sitar (2009). These motions induced nonlinear response in the sand, and measured shear strains and the interpreted modulus reduction (G/G_{max}) curve by Al Atik and Sitar were used to estimate representative values of G/G_{max} = 0.28, 0.25, and 0.10 for the SC1, SC2, and PI2 ground motions, respectively. Comparisons between computed (FD solution) and measured maximum earth pressures for the three digitized ground motions are shown in Fig. 6 for SC2 and PI2 (SC1 omitted for clarity). Resultant forces for all three motions are shown in Table 2. Resultant force errors range from -7% to +23% for the FD solution and from +6% to +23% for the SF solution. Although the earth pressure resultants are predicted quite well, the shape of the pressure distributions differ significantly, with the reported distributions from measurements increasing linearly with depth and the predicted distributions being approximately zero at the base of the wall and having their maximum at the ground surface. This mismatch may result in part from the assumption of depth-invariant k_y^i, whereas the shear modulus of sand in the centrifuge models increases with depth. A more robust solution would utilize k_y^i values that increase with depth in accordance with the variation in soil shear modulus, combined with a site response study that captures the influence of these variations on the free-field displacement profile. We lacked the required data to perform such an analysis. It should be noted that the modulus reduction was an important part of this analysis; if taken as unity (linear soil) earth pressures are significantly over-predicted.

Mononobe-Okabe earth pressures presented by Al Atik and Sitar (2009) were computed using the ground surface *PGA* and 0.65*PGA*. For consistency with the Ostadan (2005) comparisons, the PGA-based M-O estimates are presented here. As shown in Table 2, the M-O pressure resultants significantly exceed the measurements. It is helpful to visualize these results relative to the diagrams in Figure 4. If the frequency content of the motions in the centrifuge model are assumed to be dominated by site response above the essentially rigid base of the container, then $\lambda = 4D$, which produces λ/H=12. This is well to the right of the peak, and therefore anticipated soil pressures from kinematic interaction are quite small. Not surprisingly, those pressures fall below the range of M-O pressures.

The results in Figure 6 and Table 1 compare results from the proposed analysis with maximum kinematic earth pressure increments presented by Al Atik and Sitar (2009) (i.e., total earth pressure minus initial static earth pressure minus the component from inertia of the wall mass). However, Al Atik and Sitar (2009) indicate that the peak bending moments in the walls arose from a combination of kinematic and inertia loading, and peak moments were out-of-phase with peak kinematic earth pressures. The evaluation of these inertial effects is a straightforward extension of the proposed methodology, but is not considered here for brevity and because required data is unavailable.

Effect of Dynamic Modifier on Lateral Wall-Soil Stiffness Terms

Calculations of P_E presented above utilized frequency-dependent stiffness terms (Eqns. 7a and 7b) for both the FD and SF solutions. The calculations were repeated omitting the dynamic component (i.e., setting $\omega = 0$). Setting the frequency modifiers to unity increased the computed earth pressures by about 15 to 20% for the FD solution for both the Ostadan and Al Atik and Sitar cases. This generally increases model misfit to the data from the literature. Using the SF solution, comparable pressure increases for the Al Atik and Sitar case are observed, but > 200% increases are observed for the Ostadan case.

On the basis of these comparisons, until more advanced models for k_y^i and k_z^i can be developed that account for soil layering, application of the frequency-dependent terms in Eq. (7a) and (7b) is recommended when the interaction effects are strong (i.e., near the peak of the transfer functions in Figure 4, or $\lambda/H \approx 1.5$-5.0). Otherwise, for the common case of $\lambda/H > 5$, implementation of the dynamic modifier appears to be helpful but not essential.

Recommendations and Conclusions

We present a kinematic soil-structure interaction approach that provides a unifying framework to explain the lower-than-M-O seismic earth pressure increments observed by Al-Atik and Sitar (2009, 2010) and the higher-than-M-O pressure increments computed by Ostadan (2005), Veletsos and Younan (1994), and others. The approach is admittedly simplified in several respects; in particular, the effects of wall and foundation inertia are not considered (consistent with a kinematic assumption), the Winkler assumption is utilized, the single-frequency solution significantly simplifies the broadband ground motion driving the kinematic demands, soil nonlinearity can only be indirectly included using an equivalent-linear approximation, and potential impacts of alternate initial gravity-induced stress conditions (e.g., active, at-rest) on the seismic earth pressure increment are not considered. Despite those caveats, the approach is physically sound and provides a clear basis for understanding the factors driving seismic earth pressures for many practical retaining wall configurations. Additional experimental observations and numerical simulations are needed to validate the procedure for ranges of ground motion frequencies and wall configurations, evaluate the relative contributions of inertial effects, and to formulate detailed recommendations for design application. Nevertheless, the proposed approach produces estimates of seismic earth pressures that are significantly more accurate than M-O theory.

Numerical simulations are warranted for cases where the assumptions associated with the proposed method are expected to produce unacceptably large errors. Seismic earth pressures from inertial interaction should also be considered in general application, and may be the only significant source of seismic earth pressures when kinematic interaction is insignificant. Inertial demands have different origins, and as such, may be out of phase with kinematic demands.

Inertia demands should be evaluated separately using a procedure like that shown in Fig. 1b and described in detail elsewhere (e.g., NIST, 2012).

Acknowledgments

We would like to thank Farhang Ostadan for sharing the ground motion data utilized in his 2005 paper. We thank two anonymous reviewers for their comments, which have helped us to improve the paper.

References

Akkar, S. and Özen, Ö. (2005). "Effect of peak ground velocity on deformation demands for SDOF systems," *Earthquake Eng. Struct. Dyn.* 34 (13), 1551–1571.

Al Atik, L. and Sitar, N. (2009). "Experimental and analytical study of the seismic performance of retaining structures." *Rpt. No. PEER-2008/104*, Pacific Earthquake Engineering Research Center, UC Berkeley.

Al Atik, L. and Sitar, N. (2010). "Seismic earth pressures on cantilever retaining structures," *J. Geotech. & Geoenv. Eng.*, ASCE, 136 (10), 1324-1333.

Arias A, Sanchez-Sesma, F.J., Ovando-Shelley, E. (1981). "A simplified elastic model for seismic analysis of earth-retaining structures with limited displacements," *Proc. Int Conf. Recent Adv in Geotech. Eqk. Eng. & Soil Dyn.*, S Prakash, editor. Univ. of Missouri, Rolla, Vol 1, 235-240.

Bommer, J. J. and Alarcón, J. E. (2006). "The prediction and use of peak ground velocity," *J. Earthquake Eng.*, 10 (1), 1–17.

Brandenberg, S.J., Coe, J., Nigbor, R.L., and Tanksley, K. (2009). ”Different approaches for estimating ground strains from pile driving vibrations at a buried archeological site.” *J. Geotech. Geoenviron. Eng.*, 135(8), 1101–1112.

Chen, W.F. (1975). *Limit analysis and soil plasticity*. *Developments in geotechnical engineering*. Elsevier, Amsterdam, The Netherlands.

Chen, W.F, and Liu, X.L. (1990). *Limit analysis in soil mechanics*. Elsevier, Amsterdam, The Netherlands.

Elsabee, F. and Morray, J.P. (1977). “Dynamic behavior of embedded foundations,” Publication No. R77-33, MIT, Cambridge, MA.

Gazetas, G. (1983). “Analysis of machine vibrations: state of the art,” *Soil Dyn. Earthquake Eng.*, 2(1), 2-42.

Gazetas, G. (1991). “Foundation vibrations,” *Foundation Engineering Handbook*, 2nd Edition, Chapter 15, H.-Y. Fang, ed., Chapman and Hall, New York, New York.

Gazetas, G., and Roesset, J.M. (1976). “Forced vibrations of strip footings on layered soils,” in *Methods of Structural Analysis*, National Structural Engineering Conference; August 22-25, 1976, Madison, WI, WE Saul and AH Peyrol (eds.), ASCE, Vol. 1, 115-131.

Idriss, I.M., and Sun, J. I. (1991). “User’s manual for SHAKE91”, Center for Geotechnical Modeling, University of California, Davis, CA, 65 p.

Jakub, M., and Roesset, J.M. (1977). “Nonlinear stiffness of foundations.” *Research Report R77-35*, MIT, Cambridge, MA.

Kausel, E., Whitman, A., Murray, J., and Elsabee, F. (1978). “The spring method for embedded foundations,” *Nuclear Engineering and Design*, 48, 377-392.

Kloukinas, P., Langoussis, M., and Mylonakis, G. (2012). “Simple wave solution for seismic earth pressures on non-yielding walls,” *J. Geotech. & Geoenv. Eng.*, ASCE, 138 (12), 1514–1519.

Lew, M., Sitar, N. and Al-Atik, L. (2010). “Seismic earth pressures: Fact or fiction,” in *Earth Retention Conference 3*, ASCE Geotechnical Special Publication 208, R Finno, YMA Hashash, and P Arduino (eds.).

Lysmer, J., Ostadan, F., and Chin, C. (1999). SASSI2000 *Theoretical Manual*, Geotechnical Engineering Division, Civil Engineering Department, University of California, Berkeley.

Li, X. (1999). “Dynamic analysis of rigid walls considering flexible foundation.” *J. Geotech. Geoenviron. Eng.*, 125(9), 803-806.

Mononobe, N. and Matsuo, M. (1929). “On the determination of earth pressures during earthquakes.” *Proc. World Engrg. Congress*, 9, 179–187.

Mushkelishvili, N.I. (1963). “Some basic problems of the mathematical theory of elasticity.” P. Noordhoff, Groningen, The Netherlands. 714 p.

Mylonakis, G., Nikolaou, S., and Gazetas, G. (2006). “Footings under seismic loading: Analysis and design issues with emphasis on bridge foundations,” *Soil Dyn. Earthquake Eng.*, 26, 824-853.

National Cooperative Highway Research Program, NCHRP (2008). *Seismic Analysis and Design of Retaining Walls, Buried Structures, Slopes, and Embankments*. Report 611, Prepared by D.G.

Anderson, G.R. Martin, I.P. Lam, and J.N. Wang. Transportation Research Board, National Academies, Washington DC.

National Institute of Standards and Technology, NIST (2012). *Soil-Structure Interaction for Building Structures*, Report NIST GCR 12-917-21, Prepared by NEHRP Consultants Joint Venture, J.P. Stewart, Project Technical Director. US Dept. of Commerce, Gaithersburg, MD.

Okabe, S. (1924). "General theory of earth pressure and seismic stability of retaining wall and dam." *J. Japanese Society of Civil Engineering*, 12 (4), 34-41.

Ostadan, F. (2005). "Seismic soil pressure for building walls – an updated approach," *Soil Dyn. Earthquake Eng.*, 25, 785-793.

Pais, A and Kausel, E. (1988). "Approximate formulas for dynamic stiffnesses of rigid foundations," *Soil Dyn. Earthquake Eng.*, 7(4), 213-227.

Rathje, E.M., Faraj, F. Russell, S. and Bray, J.D. (2004). "Empirical relationships for frequency content parameters of earthquake ground motions," *Earthquake Spectra*, 20 (1), 119-144.

Seed, H.B. and Whitman, R.V. (1970). "Design of earth retaining structures for dynamic loads." *Proc., ASCE Specialty Conf. on Lateral Stresses in the Ground and Design of Earth Retaining Structures*, Vol. 1, pp. 103-147, Cornell Univ., Ithaca, NY.

Steedman, R.S., and Zeng, X. (1990). "The influence of phase on the calculation of pseudo-static earth pressure on a retaining wall." *Geotechnique*, 40(1), 103-112.

Trifunac, M.D., Todorovska, M.I., and Ivanović, S.S. (1996). "Peak velocities and peak surface strains during Northridge, California, earthquake of 17 January 1994," *Soil Dyn. Earthquake Eng.*, 15, 301-310.

Veletsos, A.S. and Prasad, A.M. (1989). “Seismic interaction of structures and soils: Stochastic approach,” *J. Struct. Engrg.*, 115 (4), 935–956.

Veletsos A.S. and Younan, A.H. (1994). “Dynamic soil pressures on rigid retaining walls.” *Earthquake Eng. Struct. Dyn.*, 23 (3), 275-301.

Wood, J.H. (1973). “Earthquake induced soil pressures on structures,” *Report No. EERL 73-05*, California Institute of Technology, Pasadena, CA.

List of Figure Captions

Figure 1. Schematic illustration of the kinematic and inertial interaction components of foundation-soil interaction for an embedded foundation system. FIM = Foundation Input Motion.

Figure 2. Schematic of embedded rigid strip foundation excited by vertically propagating shear wave.

Figure 3. Translational and rotational static stiffness interaction factors, χ_y and χ_{xx}, respectively, versus H/B.

Figure 4. Normalized P_E versus normalized wavelength λ/H for various contributions of wall normal stress to translational and rotational stiffness.

Figure 5. Kinematic transfer functions for translational and rotational Foundation Input Motions derived from the present study and compared to the simplified approach of Kausel et al. (1978).

Figure 6. Maximum seismic earth pressure increments computed by Ostadan (2005) and Al Atik and Sitar (2009) compared with full frequency-domain solution by the proposed kinematic methodology.

Table 1. Resultants of seismic earth pressure increments from Ostadan (2005), the Mononobe-Okabe solution, and the proposed kinematic methodology.

	Earth Pressure Resultant, P_E (kN/m)			
Ground Motion	Ostadan (2005)	FD solution	SF solution	Mononobe-Okabe Solution
Loma Prieta	414	415 (+0%)	487 (+18%)	160 (-61%)
ATC	368	341 (-7%)	461 (+25%)	160 (-57%)
RG1.60	478	451 (-6%)	588 (+23%)	160 (-67%)
EUS distant	405	362 (-11%)	637 (+57%)	160 (-60%)
EUS local	179	201 (+12%)	158 (-12%)	160 (-11%)

Table 2. Resultant of seismic earth pressure increments from Al Atik and Sitar (2009), the Mononobe-Okabe solution, and the proposed kinematic methodology.

	Earth Pressure Resultant, P_E (kN/m), (% error)			
Ground Motion	Al Atik and Sitar (2009)	FD solution	SF solution	Mononobe-Okabe solution
Loma Prieta SC1	90	110 (+23%)	95 (+6%)	180 (+100%)
Kobe PI2	146	164 (+13%)	180 (+23%)	∞ (+∞%)[1]
Loma Prieta SC2	101	94 (-7%)	121 (+20%)	235 (+132%)

[1] The M-O prediction of infinite earth pressure is caused by the inertial force exceeding the shear strength of the sand at the base of the wall, and is a well-recognized unrealistic artifact that makes the M-O theory difficult to apply in practice for sites with very strong design ground motions.

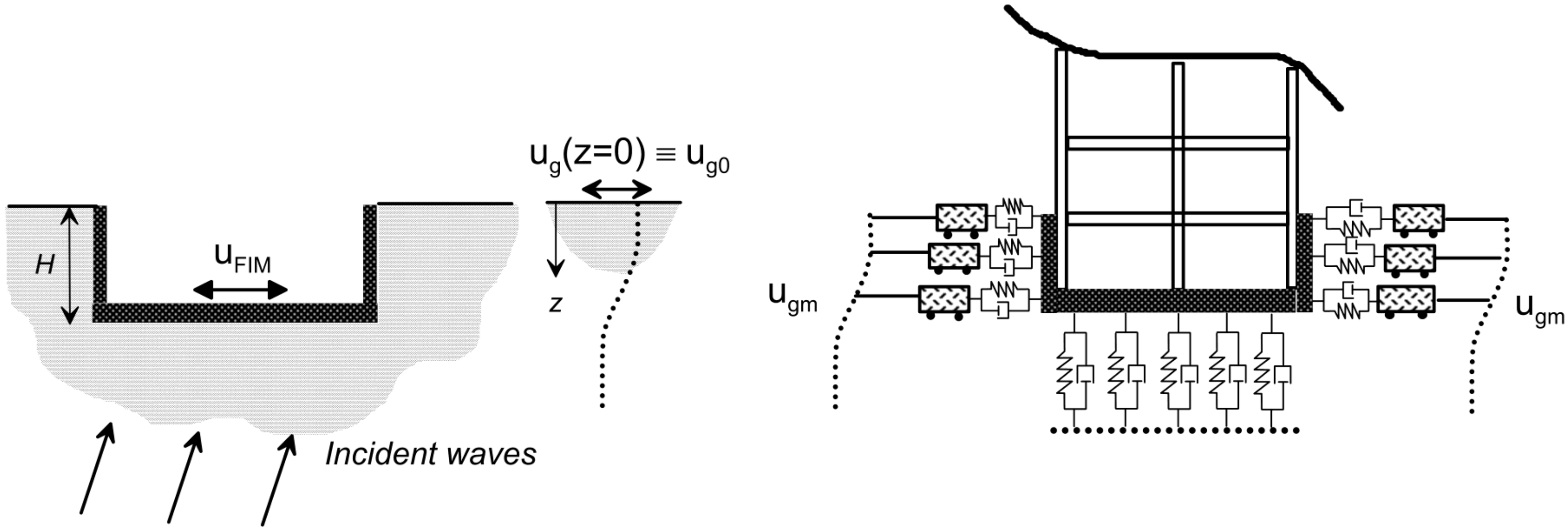

(a) (b)

Figure 1

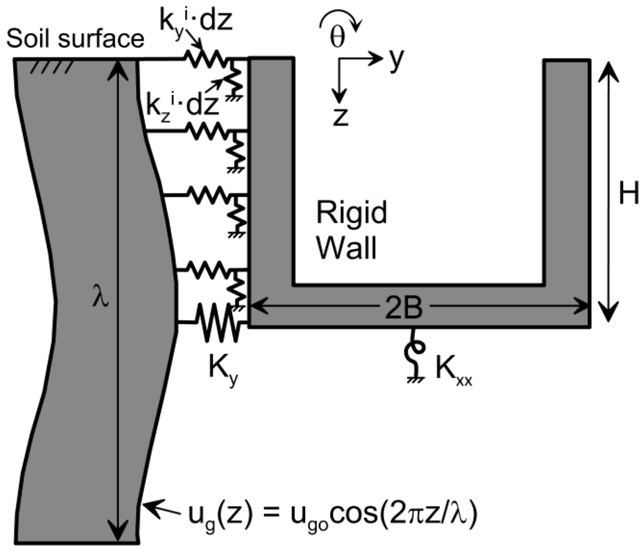

Soil surface
$k_y^i \cdot dz$
$k_z^i \cdot dz$
θ
y
z
Rigid
Wall
H
λ
2B
K_y
K_{xx}
$u_g(z) = u_{go}\cos(2\pi z/\lambda)$

Figure 2

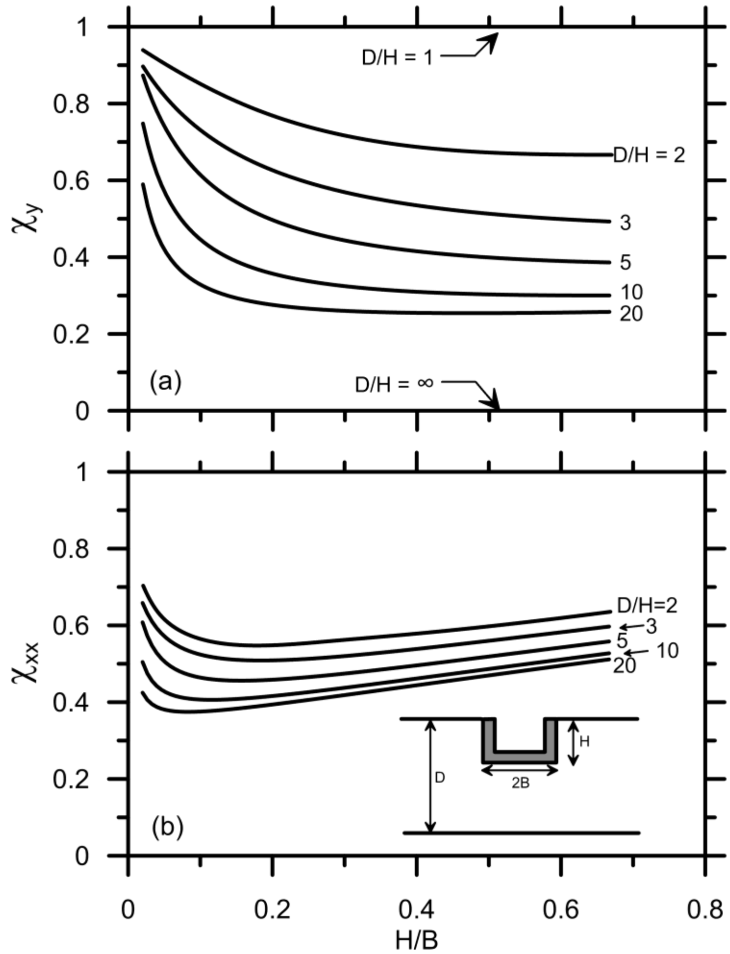

D/H = 1
D/H = 2
3
5
10
20
(a)
D/H = ∞
χ_y
D/H=2
3
5
10
20
H
D
2B
(b)
χ_{xx}
H/B
0
0.2
0.4
0.6
0.8
1

Figure 3

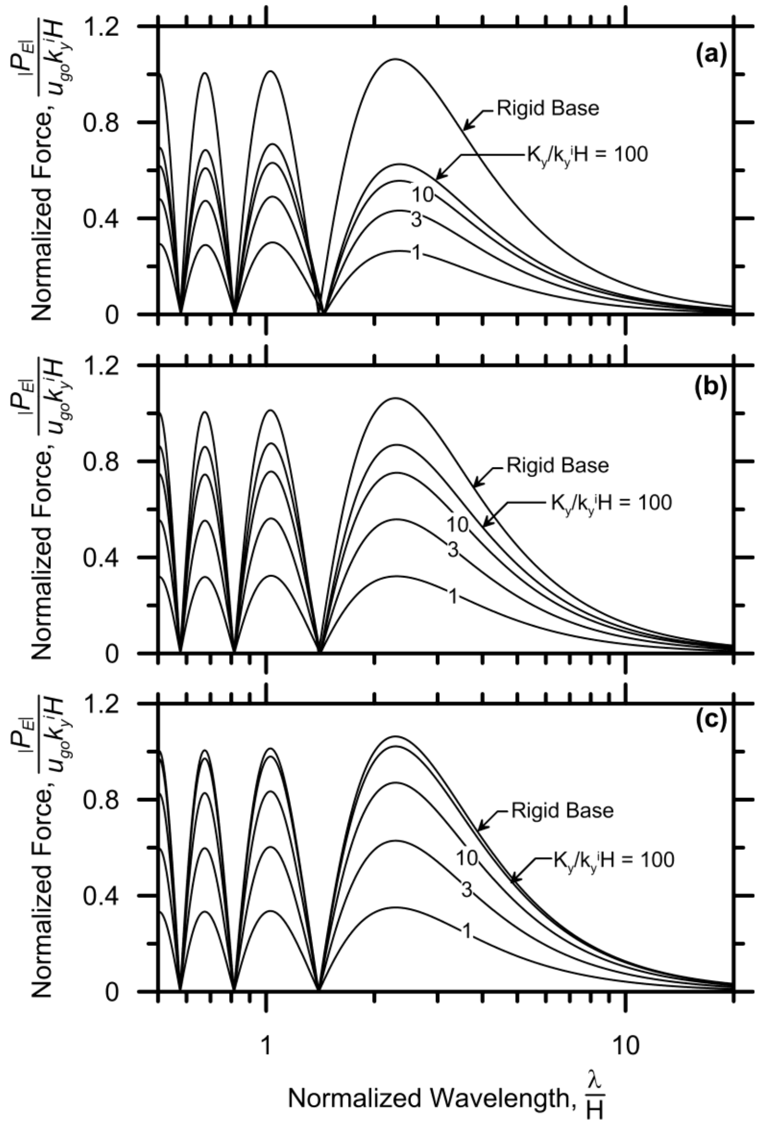
(a)
(b)
(c)
Rigid Base
Ky/kyiH = 100
10
3
1
Normalized Force, |PE|/ugokyiH
Normalized Wavelength, λ/H
0
0.4
0.8
1.2
1
10

Figure 4

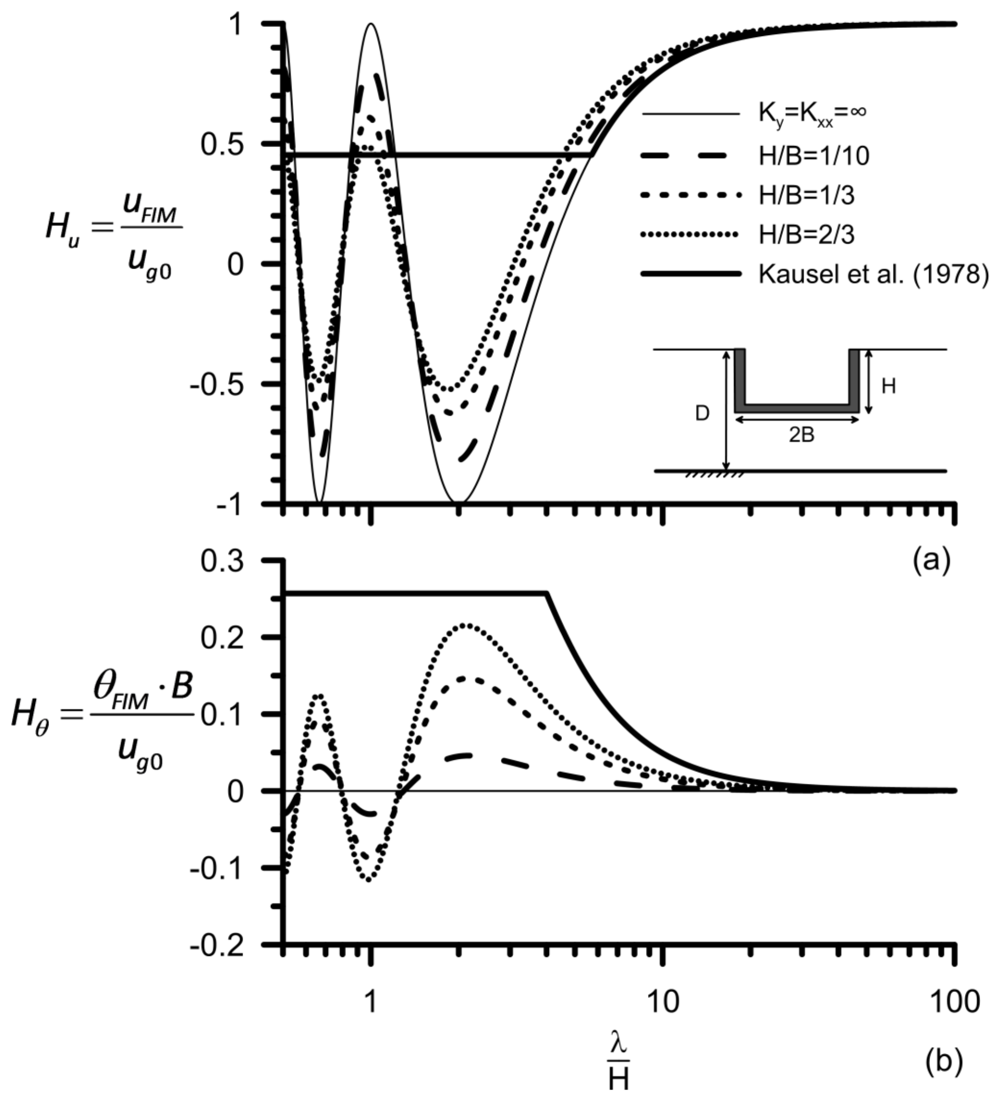
$H_u = \frac{u_{FIM}}{u_{g0}}$
$H_\theta = \frac{\theta_{FIM} \cdot B}{u_{g0}}$
$K_y = K_{xx} = \infty$
H/B=1/10
H/B=1/3
H/B=2/3
Kausel et al. (1978)
D
H
2B
(a)
(b)
$\frac{\lambda}{H}$

Figure 5

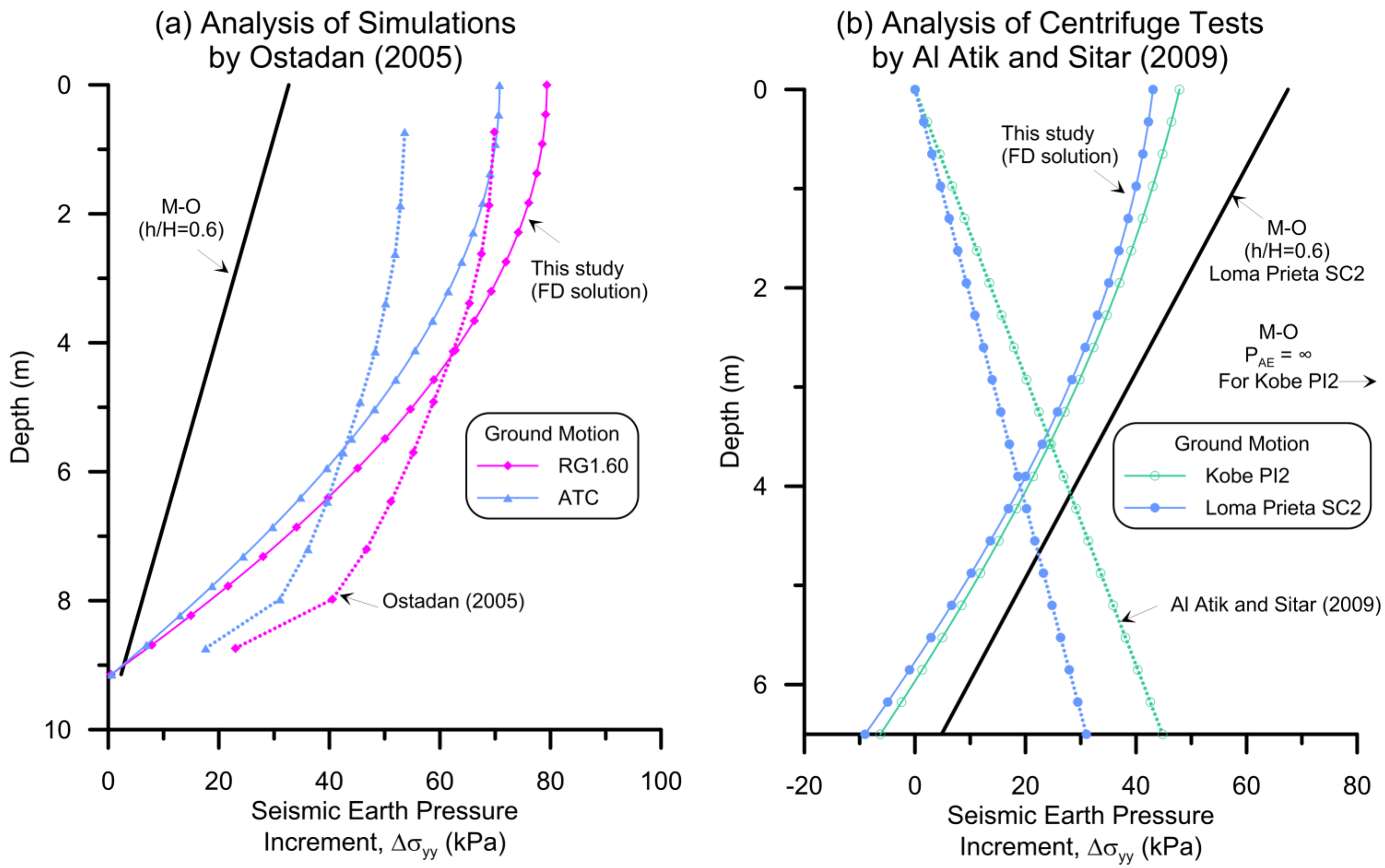
(a) Analysis of Simulations by Ostadan (2005)
M-O (h/H=0.6)
This study (FD solution)
Ostadan (2005)
Ground Motion
RG1.60
ATC
Depth (m)
Seismic Earth Pressure Increment, $\Delta\sigma_{yy}$ (kPa)
(b) Analysis of Centrifuge Tests by Al Atik and Sitar (2009)
This study (FD solution)
M-O (h/H=0.6) Loma Prieta SC2
M-O $P_{AE} = \infty$ For Kobe PI2
Ground Motion
Kobe PI2
Loma Prieta SC2
Al Atik and Sitar (2009)
Depth (m)
Seismic Earth Pressure Increment, $\Delta\sigma_{yy}$ (kPa)

Figure 6

Derivation of equation for vertical stiffness intensity k_z^i

This digital supplement presents the derivation for vertical stiffness intensity, k_z^i, for an elastic soil mass moving vertically relative to a rigid wall. The formulation follows the approach presented by Kloukinas et al. (2012) for solving k_y^i using a special integration technique inspired by the work of Vlasov and Leontiev (1966). The solution procedure assumes that the free-field soil is vibrating according to a vertical displacement field, and a vertical rigid wall alters the displacement field thereby mobilizing shear tractions at the interface between the wall and the retained soil. The free-field vertical displacement field is assumed to be known, and the horizontal variation in the vertical displacement field caused by the presence of the rigid wall is subsequently solved to render vertical force equilibrium.

Stresses shown on the hatched region in Fig. 7 represent dynamic stress increments, and we assume, following several related studies discussed in Kloukinas et al. (2012), that dynamic stresses in the horizontal direction are zero (i.e., σ_y = 0) throughout the domain, plane-strain conditions apply, and the displacement gradient $\frac{\partial u_y}{\partial z}$ is small compared to the complementary term $\frac{\partial u_z}{\partial y}$.

Equilibrium of vertical forces on the hatched region results in Eq. (A1).

$$\frac{\partial \sigma_z}{\partial z} + \frac{\partial \tau_{yz}}{\partial y} + \rho \frac{\partial^2 u_z}{\partial t^2} = 0 \tag{A1}$$

Stress-strain relations are provided in Eqs. (A2), in which *G* is shear modulus, and ν is Poisson ratio.

$$\sigma_z = -2G\left(\frac{\nu}{1-2\nu}\right)\frac{\partial u_y}{\partial y} - 2G\left(\frac{1-\nu}{1-2\nu}\right)\frac{\partial u_z}{\partial z} \tag{A2a}$$

$$\sigma_y = -2G\left(\frac{1-\nu}{1-2\nu}\right)\frac{\partial u_y}{\partial y} - 2G\left(\frac{\nu}{1-2\nu}\right)\frac{\partial u_z}{\partial z} \tag{A2b}$$

$$\tau_{yz} = -G\left(\frac{\partial u_y}{\partial z} + \frac{\partial u_z}{\partial y}\right) \tag{A2c}$$

By setting σ_y = 0, the *y*-direction displacement gradient can be expressed in terms of the vertical displacement gradient and ν, as shown in Eq. (A3).

$$\frac{\partial u_y}{\partial y} = -\frac{\nu}{1-\nu}\frac{\partial u_z}{\partial z} \tag{A3}$$

After substituting Eq. (A3) into Eq. (A2a) and taking the partial derivative with respect to *z*, taking the partial derivative of Eq. (A2c) with respect to *y*, and substituting into Eq. (A1) considering that $\frac{\partial u_y}{\partial z} = 0$, one obtains the governing equation

$$\psi_s{}^2 \frac{\partial^2 u_z}{\partial z^2} + \frac{\partial^2 u_z}{\partial y^2} + k^2 \frac{\partial^2 u_z}{\partial t^2} = 0 \tag{A4}$$

where $\psi_s = \sqrt{\frac{2-\nu}{1-\nu}}$ is a compressibility coefficient, and k = ω/V_s = wave number.

Following Kloukinas et al. (2012), we assume that the displacement field in the soil behind the wall can be written in separable form

$$u_z(y,z) = Y(y)\Phi(z) \tag{A5}$$

where *Y* is an unknown function of the horizontal variable *y*, and $\Phi(z)$ is a predetermined dimensionless function of the vertical variable that satisfies the geometric boundary condition $\Phi(H)$=0 and $\Phi(0)$=1.

To eliminate the variable *z*, Eq. (A4) is multiplied by $\Phi(z)$ and integrated over layer thickness to give

$$\psi_s{}^2 Y \int_0^H \frac{d^2\Phi}{dz^2}\Phi dz + \frac{d^2Y}{dy^2}\int_0^H \Phi^2 dz + k^2 Y \int_0^H \Phi^2 dz = 0 \tag{A6}$$

The first term on the left hand side of Eq. (A6) can be integrated by parts to obtain the weak form

$$\psi_s{}^2 Y \int_0^H \frac{d^2\Phi}{dz^2}\Phi dz = \psi_s{}^2 Y \frac{d\Phi}{dz}\Phi\Big|_0^H - \psi_s{}^2 Y \int_0^H \left(\frac{d\Phi}{dz}\right)^2 dz \tag{A7}$$

Assuming a traction-free boundary condition at the soil surface means that $\left.\frac{d\Phi}{dz}\right|_{z=0} = 0$. Combined with the condition that $\Phi(H)$=0, the first term on the right-hand side of Eq. (A7) must also be zero. By making appropriate substitutions and re-arranging terms, Eq. (A6) can be expressed as

$$\frac{d^2Y}{dy^2} - \left(\psi_s{}^2 \frac{\int_0^H \left(\frac{d\Phi}{dz}\right)^2 dz}{\int_0^H \Phi^2 dz} - k^2 \right) Y = 0 \tag{A8}$$

The general form to the solution of Eq. (A8) is

$$Y(y) = C_1 e^{y\sqrt{a_c{}^2 - k^2}} + C_2 e^{-y\sqrt{a_c{}^2 - k^2}} \tag{A9}$$

where $a_c^2 = \psi_s{}^2 \frac{\int_0^H \left(\frac{d\Phi}{dz}\right)^2 dz}{\int_0^H \Phi^2 dz}$.

Noting that Y(∞) is finite and Y(0) = u_o, one obtains $C_1 = 0$ and $C_2 = u_o$. Substitution into Eq. (A5) results in

$$u_z(y,z) = u_o e^{-y\sqrt{a_c{}^2 - k^2}} \Phi(z) \tag{A10}$$

Substituting Eq. (A10) into Eq. (A2c), the expression for shear stress is

$$\tau_{yz}(y,z) = -G\frac{\partial u_z}{\partial y} = G a_c e^{-y\sqrt{a_c{}^2 - k^2}} u_o \Phi(z) \tag{A11}$$

The vertical stiffness intensity can then be computed as

$$k_z^i = \frac{\int_0^H \tau_{yz}(y,z)dz}{\int_0^H u_z(y,z)} = \frac{u_o G\sqrt{a_c{}^2 - k^2} e^{-y\sqrt{a_c{}^2 - k^2}} \int_0^H \Phi(z)dz}{u_o e^{-y\sqrt{a_c{}^2 - k^2}} \int_0^H \Phi(z)dz} = G a_c \sqrt{1 - \left(\frac{k}{a_c}\right)^2} \tag{A12}$$

Selecting $\Phi(z) = \cos\left(\frac{\pi z}{2H}\right)$, the value of a_c can be solved as:

$$a_c = \psi_s \left(\frac{\int_0^H \frac{d^2}{dz^2} \cos\left(\frac{\pi z}{2H}\right) dz}{\int_0^H \cos\left(\frac{\pi z}{2H}\right)^2 dz} \right)^{0.5} = \sqrt{\frac{2-\nu}{1-\nu}} \frac{\pi}{2H} \tag{A13}$$

Substituting Eq. (A13) into Eq. (A12) results in the final expression for k_z^i shown in Eq. (A14) and (7b) from the main text.

$$k_z^i = \frac{\pi}{2} \sqrt{\frac{2-\nu}{1-\nu}} \frac{G}{H} \sqrt{1 - \left(\frac{2\omega H}{\pi V_s}\right)^2} \tag{A14}$$

Material damping can be incorporated into the solution for k_z^i by using the complex shear modulus, $G(1+\mathbf{i}2\xi)$, where ξ is the percent damping. For static loading conditions in which $\omega = 0$, one obtains a static stiffness shown in Eq. (A15). This equation may be appropriate when the loading frequency is much lower than the natural frequency of the soil deposit.

$$k_z^i = \frac{\pi}{2} \sqrt{\frac{2-\nu}{1-\nu}} \frac{G}{H} \tag{A15}$$

Furthermore, as frequency becomes very high, the stiffness is complex due to the negative sign of the quantity inside the square root in Eq. (A14), and the imaginary portion dominates and becomes equal to Eq. (A16) as $\omega \rightarrow \infty$.

$$k_z^i = i\omega \frac{G}{V_s} \sqrt{\frac{2-\nu}{1-\nu}} \tag{A16}$$

This indicates that the wall stiffness can be represented by a dashpot c_z^i, in accordance with elementary wave propagation theory (Eq. A17).

$$c_z^i = \rho V_s \sqrt{\frac{2-\nu}{1-\nu}} \tag{A17}$$

This suggests the existence of an equivalent propagation velocity, influenced by soil compressibility, in accordance with Eq. (A4).

References:

Kloukinas, P., Langoussis, M. and Mylonakis, G. (2012). “Simple wave solution for seismic earth pressures on non-yielding walls,” *J. Geotech. & Geoenv. Eng.*, ASCE, 138 (12), 1514–1519.

Vlasov, V.Z. and Leontiev, U.N. (1966). *Beams, plates and shells on elastic foundation*, Israel Program for Scientific Translation, Jerusalem (translated from Russian).

List of Figure Captions:

Figure 7. Schematic of vertical wall and a soil element with vertical and shear stresses.

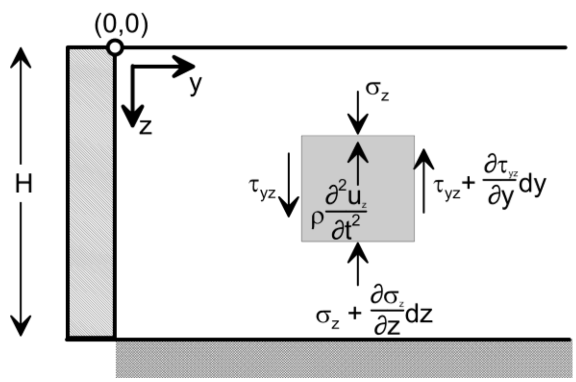

Figure 7